JACS ARTICLES

Published on Web 03/15/2010

"Two-Step" Chronoamperometric Method for Studying the Anaerobic Inactivation of an Oxygen Tolerant NiFe Hydrogenase

Vincent Fourmond, Pascale Infossi, Marie-Thérèse Giudici-Orticoni, Patrick Bertrand, and Christophe Léger*

Laboratoire de Bioénergétique et Ingénierie des Protéines, CNRS, UPR 9036, Institut de Biologie de la Méditerranée and Aix-Marseille Université, 31 Chemin Joseph Aiguier, 1 3402 Marseille Cedex 20, France

Received December 29, 2009; E-mail: christophe.leger@ifr88.cnrs-mrs.fr

Abstract: Hydrogenases catalyze the oxidation and production of H_2. The fact that they could be used in biotechnological devices if they resisted inhibition by O_2 motivates the current research on their inactivation mechanism. Direct electrochemistry has been thoroughly used in this respect but often in a qualitative manner. We propose a new and precise chronoamperometric method for studying the anaerobic inactivation mechanism of hydrogenase, which we apply to the oxygen-tolerant NiFe enzyme from *Aquifex aeolicus*. We demonstrate that the voltammetric data cannot be used for measuring the reduction potential of the so-called NiB inactive state, even in the small scan rate limit. We show that the inactivation mechanism proposed for standard (oxygen-sensitive) NiFe hydrogenases does not apply in the case of the enzyme from *A. aeolicus*. In particular, the activation and inactivation reactions cannot follow the same reaction pathway.

Introduction

Hydrogenases, the enzymes which catalyze the biological conversion between protons and dihydrogen, have been studied for about 50 years,[1] but the search for catalysts of H_2 production and oxidation[2] has recently encouraged increased activity in this research area. Hydrogenases are classified as NiFe or FeFe depending on the metal content of their active sites. They are often large and structurally complex enzymes,[3] whose active site is buried into the protein and connected to the solvent by hydrophobic cavities which guide the substrate,[4,5] a chain of iron−sulfur clusters for transferring electrons,[6] and a series of protonable amino acids and water molecules for transporting the protons[7] that can be either the product or the substrate of the reaction.

Irrespective of the application considered, whether it is hydrogen production by photosynthetic bacteria[8] or in photoelectrochemical devices,[9] or hydrogen oxidation in fuel cells,[10] a troublesome property of all hydrogenases is the fact that they are inhibited, to some extent, by oxygen. Not all hydrogenases react with O_2 in the same manner. For example EPR investigations showed that oxygen damages the FeS clusters of the FeFe hydrogenase from *Desulfovibrio desulfuricans*;[11,12] in contrast, we[13] and others[14] interpreted the observation that the FeFe hydrogenases from *Clostridium acetobutylicum* and *Chlamydomonas reinhardtii* are protected by the competitive inhibitor CO as an indication that O_2 targets the enzyme's active site. The inactivation of NiFe hydrogenases does not seem to involve the destruction of the electron transferring clusters, but it is a complex process nonetheless: in the case of the "standard" (oxygen-sensitive) NiFe hydrogenases such as those from *Allochromatium vinosum*, *Desulfovibrio gigas*, and *Des-*

(1) Cammack, R., Frey, M., Robson, R., Eds.; *Hydrogen as a fuel, learning from Nature*; Taylor and Francis: London, 2001.
(2) Le Goff, A.; Artero, V.; Jousselme, B.; Tran, P. D. D.; Guillet, N.; Métayé, R.; Fihri, A.; Palacin, S.; Fontecave, M. *Science* **2009**, *326*, 1384–1387.
(3) Fontecilla-Camps, J. C.; Volbeda, A.; Cavazza, C.; Nicolet, Y. *Chem. Rev.* **2007**, *107*, 4273–4303.
(4) Leroux, F.; Dementin, S.; Burlat, B.; Cournac, L.; Volbeda, A.; Champ, S.; Martin, L.; Guigliarelli, B.; Bertrand, P.; Fontecilla-Camps, J.; Rousset, M.; Léger, C. *Proc. Natl. Acad. Sci. U.S.A.* **2008**, *105*, 11188–11193.
(5) Liebgott, P.-P.; Leroux, F.; Burlat, B.; Dementin, S.; Baffert, C.; Lautier, T.; Fourmond, V.; Ceccaldi, P.; Cavazza, C.; Meynial-Salles, I.; Soucaille, P.; Fontecilla-Camps, J. C.; Guigliarelli, B.; Bertrand, P.; Rousset, M.; Léger, C. *Nat. Chem. Biol.* **2010**, *6*, 63–70.
(6) Dementin, S.; Belle, V.; Bertrand, P.; Guigliarelli, B.; Adryanczyk-Perrier, G.; Delacey, A.; Fernandez, V. M.; Rousset, M.; Léger, C. *J. Am. Chem. Soc.* **2006**, *128*, 5209–5218.
(7) Dementin, S.; Burlat, B.; de Lacey, A. L.; Pardo, A.; Adryanczyk-Perrier, G.; Guigliarelli, B.; Fernandez, V. M.; Rousset, M. *J. Biol. Chem.* **2004**, *279*, 10508–10513.
(8) Ghirardi, M. L.; Dubini, A.; Yu, J.; Maness, P.-C. *Chem. Soc. Rev.* **2009**, *38*, 52–61.
(9) Hambourger, M.; Gervaldo, M.; Svedruzic, D.; King, P. W.; Gust, D.; Ghirardi, M.; Moore, A. L.; Moore, T. A. *J. Am. Chem. Soc.* **2008**, *130*, 2015–2022.
(10) Vincent, K. A.; Parkin, A.; Armstrong, F. A. *Chem. Rev.* **2007**, *107*, 4366–4413.
(11) Pierik, A. J.; Hagen, W. R.; Redeker, J. S.; Wolbert, R. B. G.; Boersma, M.; Verhagen, M.; Grande, H. J.; Veeger, C.; Mutsaers, P. H. A.; Sands, R. H.; Dunham, W. R. *Eur. J. Biochem.* **1992**, *209*, 63–72.
(12) Pereira, A. S.; Tavares, P.; Moura, I.; Moura, J. J. G.; Huynh, B. H. *J. Am. Chem. Soc.* **2001**, *123*, 2771–2782.
(13) Baffert, C.; Demuez, M.; Cournac, L.; Burlat, B.; Guigliarelli, B.; Bertrand, P.; Girbal, L.; Léger, C. *Angew. Chem., Int. Ed.* **2008**, *47*, 2052–2054.
(14) Stripp, S. T.; Goldet, G.; Brandmayr, C.; Sanganas, O.; Vincent, K. A.; Haumann, M.; Armstrong, F. A.; Happe, T. *Proc. Natl. Acad. Sci. U.S.A.* **2009**, *106*, 17331–17336.

10.1021/ja910685j

ulfovibrio fructosovorans, exposure to O_2 converts the active site into a mixture of fully oxidized inactive species, whose spectroscopic signatures were termed NiA and NiB in the 1980s. The NiB state can be obtained upon oxidizing the enzyme under anaerobic conditions, whereas exposure to O_2 leads to a mixture of NiA and NiB states. The inactive states can be reactivated by reduction, NiB much more quickly than NiA, hence their qualification as "ready" and "unready", respectively.[15−18] Their structure is still debated. NiB appears to be a $Ni^{III}FeOH$ form, in which a hydroxo bridges the Ni and the Fe. An oxygenated ligand, possibly a peroxo,[18−20] is also present in the NiA state. The complexity of the mechanism of aerobic inactivation, and the fact that whether an enzyme "resists" O_2 also depends on its rate of reductive reactivation, are the reasons that there can be no unique measure of the oxygen sensitivity of hydrogenases.

A few NiFe hydrogenases which have a reasonably high turnover rate even in the presence of O_2 have been identified and called "oxygen-tolerant". These include the membrane bound NiFe hydrogenases from *Ralstonia eutropha*[21,22] and *Aquifex aeolicus*.[23,24] Unlike standard hydrogenases, recent results have shown that both the aerobic and anaerobic inactivations of these "oxygen tolerant" hydrogenases lead to the same inactive state (rather than a mixture).[22] This state has a standard NiB spectral signature, but it reactivates much faster than in standard hydrogenases. It has been proposed that this is because its reduction is thermodynamically more favorable than in standard enzymes.[22]

Over the last 10 years, the technique called protein film voltammetry (PFV) has given a wealth of information on the catalytic and inhibition mechanisms of hydrogenases.[25,10] In this technique, the enzyme is adsorbed onto an electrode in a configuration which favors direct electron transfer, and the turnover frequency is simply monitored as a current. PFV is ideal for studying redox-dependent (in)activation processes, because the redox state of the enzyme can respond to changes in electrode potential, while the activity is continuously measured. In addition, in contrast to traditional solution assays, the presence of oxygen does not interfere with the activity measurement.[5,13,26,22,24]

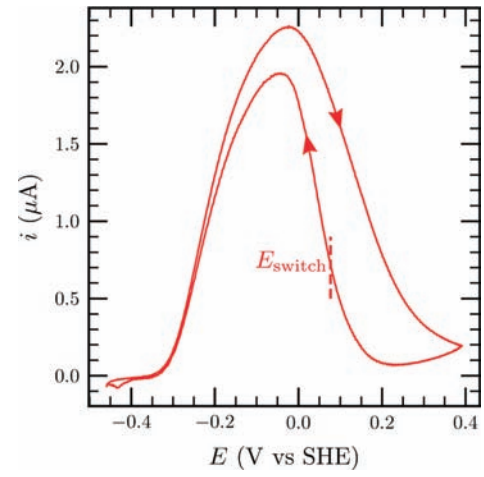

Figure 1. Cyclic voltammogram (CV) *A. aeolicus* NiFe hydrogenase adsorbed onto a rotating disk electrode, at pH7, 40 °C, under 1 atm. H_2. Electrode rotation rate 4 krpm, scan rate $\upsilon = 0.3$ mV/s. The arrows indicate the direction of the sweeps. The decrease in hydrogen oxidation activity at high potential results from the reversible formation of the NiB, inactive state.

For studying the anaerobic activation/inactivation process, two main electrochemical experiments have been carried out. One consists in sweeping the electrode potential up and down; the result is usually displayed as a plot of current against electrode potential (a cyclic voltammogram, CV). This is examplified in Figure 1, where the arrows indicate the direction of the scan. The shape of the CV is complex because the change of activity results from two antagonist contributions: increasing the electrode potential (and the driving force for H_2 oxidation) increases the turnover rate of the fully active enzyme, but it also drives the oxidative formation of NiB, and this decreases the fraction of active enzyme.[17,27] The activity of the enzyme is recovered as the potential is swept toward negative values, on the return scan. The scan rate υ, in units of V/s, is a crucial experimental parameter, because the fact that the (in)activation process is slow on the voltammetric time scale makes the current response depart from steady-state.

Limoges and Savéant have proposed a numerical procedure for calculating current responses like that in Figure 1, in the framework of a reaction scheme which depicts the interconversion between four active and inactive states of the enzyme.[27] They confirmed that the appearance of the inverted peak on the reverse scan provides a diagnostic criterion for the redox reactivation process. They found that the dimensionless governing parameters contain the ratio of the (in)activation rate constants and scan rate. No fitting of actual data was attempted, because the authors acknowledged that a realistic treatment of the system would require the evaluation of far too many parameters.

Armstrong and co-workers emphasized that a meaningful parameter can be simply measured from these complex voltammograms: it is the parameter E_{switch}, defined as the position of the first inflection point on the scan toward low potential (E_{switch} is marked by a vertical line in Figure 1).[17] This was used as a qualitative criterion to compare the ease with which different hydrogenases from various organisms reactivate after

(15) Fernandez, V. M.; Hatchikian, E. C.; Cammack, R. *Biochim. Biophys. Acta* **1985**, *832*, 69–79.
(16) Fernandez, V. *Biochim. Biophys. Acta* **1986**, *883*, 145–154.
(17) Jones, A.; Lamle, S.; Pershad, H.; Vincent, K.; Albracht, S.; Armstrong, F. *J. Am. Chem. Soc.* **2003**, *125*, 8505–8514.
(18) Lamle, S. E.; Albracht, S. P. J.; Armstrong, F. A. *J. Am. Chem. Soc.* **2004**, *126*, 14899–909.
(19) Ogata, H.; Hirota, S.; Nakahara, A.; Komori, H.; Shibata, N.; Kato, T.; Kano, K.; Higuchi, Y. *Structure* **2005**, *13*, 1635–1642.
(20) Volbeda, A.; Martin, L.; Cavazza, C.; Matho, M.; Faber, B. W.; Roseboom, W.; Albracht, S. P. J.; Garcin, E.; Rousset, M.; Fontecilla-Camps, J. C. *J. Biol. Inorg. Chem.* **2005**, *10*, 239–249; erratum 2005, *10*, 591.
(21) Vincent, K. A.; Cracknell, J. A.; Lenz, O.; Zebger, I.; Friedrich, B.; Armstrong, F. A. *Proc. Natl. Acad. Sci. U.S.A.* **2005**, *102*, 16951–16954.
(22) Cracknell, J. A.; Wait, A. F.; Lenz, O.; Friedrich, B.; Armstrong, F. A. *Proc. Natl. Acad. Sci. U.S.A.* **2009**, *106*, 20681–20686.
(23) Luo, X.; Brugna, M.; Tron-Infossi, P.; Giudici-Orticoni, M.; Lojou, E. *J. Biol. Inorg. Chem.* **2009**, *14*, 1275–1288.
(24) Pandelia, M.-E. [NiFe] hydrogenases from Desulfovibrio vulgaris Miyazaki F and Aquifex aeolicus studied by FTIR, EPR and electrochemical techniques: Redox intermediates. *O_2/CO sensitivity and light-induced effects*, Thesis, Technical University Berlin: Berlin, 2009.
(25) Léger, C.; Bertrand, P. *Chem. Rev.* **2008**, *108*, 2379–2438.
(26) Léger, C.; Dementin, S.; Bertrand, P.; Rousset, M.; Guigliarelli, B. *J. Am. Chem. Soc.* **2004**, *126*, 12162–72.
(27) Limoges, B.; Savéant, J.-M. *J. Electroanal. Chem.* **2004**, *562*, 43–52.

anaerobic inactivation.[28,22] In mechanistic studies, this parameter was given thermodynamic significance: it has been interpreted as the reduction potential of the NiB species, plotted in Pourbaix diagrams to deduce acidity constants, and its dependence on temperature has been analyzed to measure entropies and enthalpies.[17] We shall see that the results herein do not support this interpretation.

To avoid the intricacy of time and potential that is inherent to the voltammetric experiment, a second, apparently simpler electrochemical approach consists in monitoring the relaxation of the current after the potential has been stepped up (to inactivate the enzyme) or down (to force activation). Since the current is proportional to the instant concentration of active enzyme, the transients can be interpreted using a very simple scheme which connects the active and inactive forms of the enzyme

$$\text{active} \underset{k_A(E)}{\overset{k_I(E)}{\rightleftharpoons}} \text{inactive} \tag{1}$$

where $k_A(E)$ and $k_I(E)$ are the activation and inactivation rate constants, respectively. That the fraction of active enzyme changes upon stepping the electrode potential implies that k_I and/or k_A depend on potential. The information about the (in)activation mechanism can be obtained by analyzing the dependence of k_A and k_I on potential, T, pH, H_2 concentration, etc.[17] The interpretation of such kinetic data would be straightforward if the (in)activation were irreversible,[29] but it is not, and a complication therefore arises from the fact that fitting the current responses to exponential functions only yields the sum $k_A(E) + k_I(E)$, rather than $k_A(E)$ or $k_I(E)$;[30] this point has sometimes been overlooked.

In this paper, we propose a simple "two-step" chronoamperometric method for measuring both the activation and inactivation rate constants, which we apply to the oxygen tolerant NiFe hydrogenase from *A. aeolicus*. We determine the dependence of k_I and k_A on E and various other experimental parameters. We use this fresh information in a semiempirical treatment of the voltammetry, which makes it possible to simulate the CVs. We test the robustness and examine the meaning of the parameter E_{switch}, which appears to be defined by the kinetics of activation and the scan rate. We conclude that although the rate of reactivation depends on the reduction potential of NiB, this thermodynamic parameter cannot be determined from the electrochemical data alone.

We show that the knowledge of the dependences on E of both k_A and k_I restrains the mechanistic models of (in)activation, whereas the sum of the two is not discriminating. Regarding oxygen-sensitive NiFe hydrogenases, it has been shown that inactivation proceeds according to a "CE" mechanism, whereby a chemical step (probably the binding of a ligand derived from water) precedes the oxidation, and determines the rate of the overal reaction.[17] We show that this "CE" model cannot describe the (in)activation kinetics of *A. aeolicus* hydrogenase, and we propose another reaction scheme that is fully consistent with both the electrochemical data and the recent FTIR results on the same enzyme.

Results and Discussion

Two-Step Method for Determining the Activation and Inactivation Rate Constants. We derive the equation giving the fraction of active enzyme ($A(t)$) during the transient that follows a step to a potential E. $A(t)$ obeys

$$dA/dt = -k_I(E)A(t) + k_A(E)(1 - A(t)) \tag{2}$$

Solving eq 2 for constant E gives

$$A(t) = [A_0 - A_\infty(E)] \exp[-k_{tot}(E)t] + A_\infty(E) \tag{3}$$

where $A_0 = A(t = 0)$ is the initial fraction of the enzyme in the active state, $A_\infty(E)$ is the asymptotic value of A, and $1/k_{tot}(E)$ is the time constant of the exponential relaxation toward steady-state

$$A_\infty(E) = \frac{k_A(E)}{k_I(E) + k_A(E)} \tag{4a}$$

$$k_{tot}(E) = k_I(E) + k_A(E) \tag{4b}$$

This is the classical treatment of relaxation experiments in transient-state kinetics (e.g., temperature-jump or pressure-jump).[30,31]

Before we use the above equations in a quantitative manner, we call attention to a few important points:

(i) whether the enzyme activates or inactivates at a given potential depends solely on the sign of $(A_0 - A_\infty(E))$: activation and inactivation can be observed at any potential, depending on sample history;

(ii) the asymptotic fraction of active enzyme, $A_\infty(E)$, is independent of sample history;

(iii) the apparent rate constant of the exponential relaxation is neither the true inactivation rate constant k_I nor the true activation rate constant k_A: it is the sum of the two, regardless of whether the enzyme is activating or inactivating.

Provided the process is very slow on the time scale of turnover, the catalytic current is simply the time-dependent fraction of enzyme that is in the active form times the steady-state current response of the active enzyme at potential E

$$i(t) = A(t)i_A(E) \tag{5}$$

where $i_A(E) = 2FS\Gamma k_{cat}(E)$, $S\Gamma$ is the quantity of enzyme adsorbed on the electrode, and $k_{cat}(E)$ is the potential-dependent turnover rate of the fully active enzyme;[32,33] we count as positive an oxidation current.

Combining eqs 3 and 5 gives the equation for the current transient at constant E

$$i(t) = (i_0 - i_\infty) \exp[-k_{tot}(E)t] + i_\infty \tag{6}$$

We note $i_\infty = i_A(E)A_\infty(E)$ and $i_0 = i_A(E)A_0$. Fitting an exponential relaxation to the chronoamperometric data yields i_∞, i_0, and k_{tot}. These parameters can be combined to deduce $k_A(E)$ and $k_I(E)$ *on the condition that the initial value of A, A_0, is known*:

(28) Vincent, K. A.; Parkin, A.; Lenz, O.; Albracht, S. P. J.; Fontecilla-Camps, J. C.; Cammack, R.; Friedrich, B.; Armstrong, F. A. *J. Am. Chem. Soc.* **2005**, *127*, 18179–18189.
(29) Fourmond, V.; Burlat, B.; Dementin, S.; Arnoux, P.; Sabaty, M.; Boiry, S.; Guigliarelli, B.; Bertrand, P.; Pignol, D.; Léger, C. *J. Phys. Chem. B* **2008**, *112*, 15478–15486.
(30) Fourmond, V.; Sabaty, M.; Arnoux, P.; Bertrand, P.; Pignol, D.; Léger, C. *J. Phys. Chem. B* **2010**, *114*, 3341–3347.
(31) Cornish-Bowden, A. *Fundamental of Enzyme kinetics*; Portland Press: Seattle, WA, 2004.
(32) Léger, C.; Jones, A. K.; Roseboom, W.; Albracht, S. P. J.; Armstrong, F. A. *Biochemistry* **2002**, *41*, 15736–15746.
(33) Léger, C.; Jones, A. K.; Albracht, S. P. J.; Armstrong, F. A. *J. Phys. Chem. B* **2002**, *106*, 13058–13063.

$$k_A(E) = A_0 \frac{i_\infty}{i_0} k_{tot}(E) \quad (7a)$$

$$k_I(E) = k_{tot}(E) - k_A(E) \quad (7b)$$

Therefore, for determining $k_A(E)$ and $k_I(E)$, a very simple method consists in fully activating the adsorbed hydrogenase by poising the electrode at a low potential so that $A_0 = 1$; then step the potential up, and fit the current transient to eq 6 to measure the initial current i_0, the relaxation rate $k_{tot}(E)$ and the final current i_∞; then use eqs 7. However, this method is accurate only if the potential is high enough that the magnitude of the inactivation is significant; for example, in the case of *A. aeolicus* hydrogenase, we found that this "one-step" method gives correct results for $E > 0.15$ V at pH 6. Unfortunately, it is not possible to measure the two rate constants at a low potential by analyzing the reactivation that follows a single step down, because there is no potential at which the enzyme is fully inactive and therefore the value of A_0 after an initial poise at high potential is unknown. The trick of the two-step method we propose below is to determine the value of A at a high potential from the magnitude of the current transient that precedes the potential step down.

The two-step sequence is defined in Figure 2. It consists in poising the electrode at a value $E = E_0$, a conditioning potential where the enzyme is eventually fully active; then step the potential to a value E_1 that is high enough that the enzyme significantly inactivates; then step the potential down to E_2 to induce reactivation. A_0 equates 1, and the value of $A_1 = A_\infty(E_1)$ can be computed from eq 3. We include an equilibration time τ_{eq} at E_1 to let the capacitive current decrease before the current is monitored. Figure 2 shows the evolution over time of $A(t)$ and $i(t)$. We note that the former varies continuously but the step to E_2 at $t = t_2$ results in an instant change of the current due to an instant change in $i_A(E)$.

In PFV experiments, film loss always contributes to the decrease in current. To derive the equations below, we have therefore assumed that the coverage of enzyme decreases exponentially with time,[34] with a rate constant $k_/$ that may depend on electrode potential.

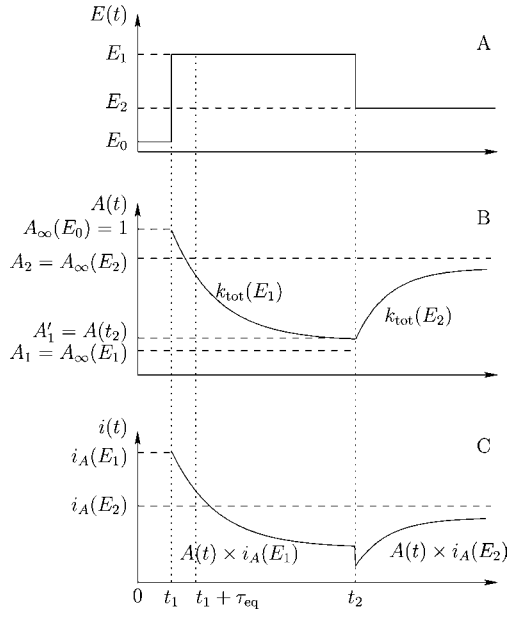

Figure 2. Schematic representation of the evolution of $A(t)$ and $i(t)$ in a typical two-step experiment (see text). The trace for $A(t)$ is continuous, but $i(t)$ instantly changes upon stepping the potential because the activity of the enzyme depends on E.

When the potential is stepped as shown in Figure 2, each current transient is entirely defined by three or four independent parameters, depending on whether or not film loss affects the signal. Indeed, the data recorded after the step to E_1 can be fitted to

$$i(t_1 < t < t_2) = i_A(E_1)\{A_1 + [1 - A_1] \times \exp[-k_{tot}(E_1)(t - t_1)]\} \exp[-k_/(E_1)(t - t_1)] \quad (8)$$

by adjusting the prefactor $i_A(E_1)$, the rate constant of the inactivation, $k_{tot}(E_1)$, the steady-state fraction of active enzyme at E_1, $A_1 = A_\infty(E_1)$, and, if necessary, the rate constant that describes film loss, $k_/(E_1)$. The parameters $k_{tot}(E_1)$ and A_1 can then be used to calculate $k_A(E_1)$ and $k_I(E_1)$ using eqs 7 with $A_0 = 1$ and $i_\infty/i_0 = A_1$.

At $t = t_2$, the fraction of the film remaining on the electrode is $\gamma_0 = \exp[-k_/(E_1)(t_2 - t_1)]$ and the fraction of active enzyme is

$$A_1' = A(t_2) = A_1 + (1 - A_1) \exp[-k_{tot}(E_1)(t_2 - t_1)] \quad (9)$$

After the potential is stepped to E_2, the enzyme reactivates according to

$$i(t > t_2) = \gamma_0 i_A(E_2)\{A_2 + [A_1' - A_2] \times \exp[-k_{tot}(E_2)(t - t_2)]\} \exp[-k_/(E_2)(t - t_2)] \quad (10)$$

We note $A_2 = A_\infty(E_2)$. This equation also depends on 4 parameters: the product $\gamma_0 i_A(E_2)$, $k_{tot}(E_2)$, A_2, and $k_/(E_2)$. The values of $k_A(E_2)$ and $k_I(E_2)$ can be deduced from $k_{tot}(E_2)$ and A_2 using eqs 7 with $i_\infty/i_0 = A_2/A_1'$ and the value of A_1' given by eq 9.

The sequence of potential steps can then be repeated, changing the values of E_1 and/or E_2, to obtain the dependence of k_A and k_I on E.

Application to *A. aeolicus* NiFe Hydrogenase. We used this two-step method to study the reversible anaerobic inactivation of *A. aeolicus* hydrogenase. We repeated the potential-step sequence for various values of E_1, keeping $E_1 - E_2$ constant. We found that a few seconds in open circuit, at $E \approx -0.35$ V, were enough to ensure full reactivation before recording each chronoamperogram (that is $A_0 = 1$). Values of $E_1 - E_2$ in the range 100−200 mV were a good compromise: it is large enough that the enzyme significantly reactivates when the potential is stepped down and small enough that fast relaxations are not hidden by excessive capacitive currents. A typical chronoamperogram is shown in Figure 3. The dotted line represents a fit to the data using eqs 8 and 10; the residuals (data minus best fit) in panel C are very small and random. The rate constants that describe film loss are more than an order of magnitude smaller than k_{tot}, therefore all 8 parameters are unambiguously determined.

This method permitted us to obtain the values of $k_I(E)$ and $k_A(E)$ for a wide range of conditions (potential, pH, hydrogen concentration). The results collected in Figure 4 (squares for

(34) Fourmond, V.; Lautier, T.; Baffert, C.; Leroux, F.; Liebgott, P.-P.; Dementin, S.; Rousset, M.; Arnoux, P.; Pignol, D.; Meynial-Salles, I.; Soucaille, P.; Bertrand, P.; Léger, C. *Anal. Chem.* **2009**, *81*, 2962–2968.

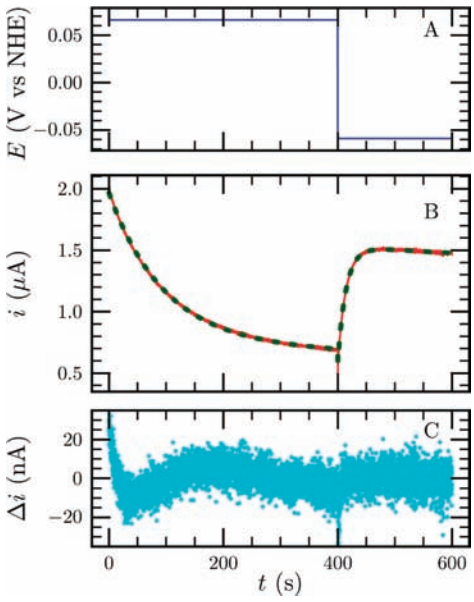

Figure 3. Typical chronoamperogram illustrating the application of the two-step method to *A. aeolicus* hydrogenase. Panel A shows electrode potential against time. Panel B shows the current obtained by subtracting the capacitive current recorded from a "blank" (as illustrated in Supporting Information, Figure S1). The green trace is the fit to eqs 8 and 10. Panel C shows the difference between the data and the fit. Experimental conditions: pH 8, $E_1 = 65$ mV, $E_2 = -60$ mV, 1 atm. of H_2, $\omega = 4$ krpm, 40 °C. The best fit was obtained with the parameters: $i_A(E_1) = 2.3\ \mu$A, $k_I(E_1) = 6.8 \times 10^{-3}\ s^{-1}$, $k_A(E_1) = 3.5 \times 10^{-3}\ s^{-1}$, $k_{/}(E_1) = 3 \times 10^{-4}\ s^{-1}$, $i_A(E_2) = 1.9\ \mu$A, $k_I(E_2) = 6.7 \times 10^{-3}\ s^{-1}$, $k_A(E_2) = 6.1 \times 10^{-1}\ s^{-1}$, and $k_{/}(E_2) = 2 \times 10^{-4}\ s^{-1}$. The initial current is lower than 2.3 μA because of the 20 s equilibration at E_1.

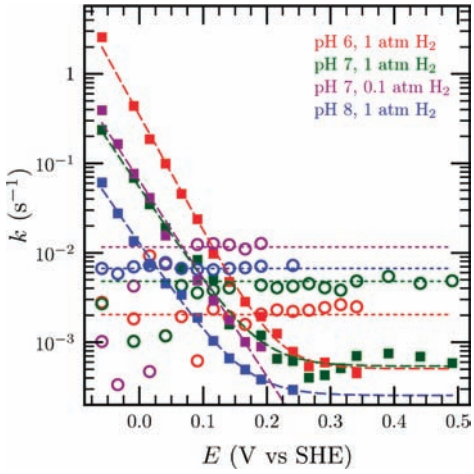

Figure 4. Variation of activation and inactivation rate constants as a function of potential, pH and hydrogen pressure. Open circles show the values of k_I, filled squares are the corresponding values of k_A. The dashed lines are the fits of k_A to eq 12. Red, green, and blue traces correspond to pH values of respectively 6, 7, and 8 for a H_2 pressure of 1 atm; purple traces show the data recorded at pH 7 and 0.1 atm. of H_2. Other conditions: 40 °C, $\omega = 4$ krpm. The scatter of values of k_I in the low potential range is due to k_A being much greater than k_I.

k_A, circles for k_I) show that k_I is essentially independent of potential

$$k_I(E) = \text{constant} \tag{11}$$

whereas k_A decreases exponentially when the potential increases until it reaches a limiting value at high potential. The decrease in k_I at low potentials is not real: the data points are scattered in this region because k_I is much lower than k_A and cannot be accurately determined. In Figure 4, the fits of the values of k_A to

$$k_A = k_0 e^{-\alpha f(E-E^0)} + k_{A\,\mathrm{lim}} \tag{12}$$

with $f = F/RT$, returned α between 0.66 (for pH 7 and 8) and 0.8 (pH 6). From eq 12, it is clear that the parameters k_0 and E^0 cannot be determined separately; only the product $k_0 \exp(\alpha f E^0)$ can. Therefore, the dependence of the rate constants on potential is governed by a thermodynamic parameter (E^0) that cannot be unambiguously determined from the electrochemical data.

Before discussing the mechanistic implications of the data in Figure 4, we first show that they can be used to simulate the voltammograms.

Simulation of the Voltammetric Response. We propose an approach distinct from that of Limoges and Savéant:[27] instead of deriving the current equations from a kinetic scheme, we use a semiempirical method. The current being given by the product $A(t)i_A(E)$ (eq 5), our strategy consists in (i) determining $A(t)$ by using the (in)activation rates in Figure 4, and (ii) determining the steady-state current response $i_A(E)$ by extrapolating the current response observed at low potential.

(i) eq 2 rules the evolution of the fraction of active enzyme over time, and we note that if E is swept, $k_I(E)$ and $k_A(E)$ depend on time. We employed standard numerical procedures to obtain $A(t)$ from eq 2, by using the functions $k_I(E)$ and $k_A(E)$ determined by the two-step method (Figure 4), together with $E =$ constant $\pm vt$ (v is the scan rate).

(ii) We obtained $i_A(E)$ by fitting the low potential part of the voltammogram, where the enzyme is actually fully active, using the equation derived in ref 35

$$i_A(E) = \frac{i_{\mathrm{lim}}}{\beta d_0 a} \ln \frac{a+b}{a} \tag{13}$$

$$a = 1 + e^{f(E^0_{OH}-E)}(1 + e^{f(E^0_{HR}-E)}) \tag{14}$$

$$b = \frac{k_2}{k_0^{\max}}[e^{f/2(E^0_{HR}-E)} + e^{f/2(E^0_{OH}-E)}(1 + e^{f(E^0_{HR}-E)})] \tag{15}$$

with $f = F/RT$. This equation gives the steady-state response of an enzyme adsorbed onto an electrode with a uniform distribution of orientations,[35] as a function of four independent parameters: E^0_{OH} and E^0_{HR} are the reduction potentials of the oxidized/half-reduced (NiSi/NiC) and half-reduced/reduced (NiC/NiR) states of the active site; the ratio $k_2/k_0^{\max}$ compares the rate of catalysis to the rate of interfacial electron transfer; the prefactor $i_{\mathrm{lim}}/\beta d_0$, which is the ratio of the limiting current over a parameter that describes the dispersion of interfacial electron transfer rate constants, βd_0.[36]

A simulation is shown in figure 5. The agreement between the calculated and experimental voltammograms is excellent, considering that the parameters defining the (in)activation have been obtained from the two-step method (the data in Figure 4)

(35) Léger, C.; Jones, A. K.; Albracht, S. P. J.; Armstrong, F. A. *J. Phys. Chem. B* **2002**, *106*, 13058–13063.

(36) β is a decay constant for the dependence of electron transfer rate on distance, and d_0 characterizes the width of the probability function of distance between the electrode and the relay that is the exit point of electrons at the enzyme surface. Only the combination $i_{\mathrm{lim}}/\beta d_0$ (not the three parameters independently) needs to be determined.

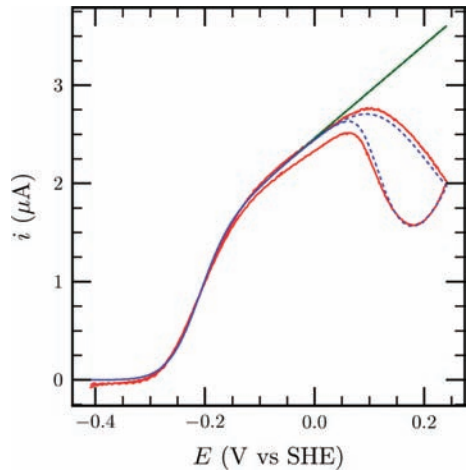

Figure 5. Cyclic voltammogram of adsorbed *A. aeolicus* hydrogenase at a small scan rate (0.3 mV/s) (solid red), and the corresponding fit (dashed blue). The green line is the voltammogram calculated by using the (in)activation rate constants obtained using the "two-step" method; the parameters describing the wave shape ($i_A(E)$) are deduced from a fit of eq 13 to the lower potential range of the voltammogram; the blue line is the corresponding value of $i_A(E)$. Conditions: pH 6, 40 °C, 1 atm. of H_2, ω = 4 krpm. Parameters: $k_I = 2.3 \times 10^{-3}$ s^{-1}, k_A given by eq 12 with $\alpha = 0.80$, $k_0 \exp \alpha f E^0 = 0.34$ s^{-1} and $k_{A\,lim} = 5 \times 10^{-4}$ s^{-1}, and the parameters describing the wave shape: $E^0_{OH} = -0.224$ V, $E^0_{HR} = -0.292$ V, $k_2/k_0^{max} = 1.2 \times 10^{-2}$, and $i_{lim}/\beta d_0 = 0.3$ μA. Film loss was neglected.

and used "as is", and only the four parameters that define the activity have been adjusted here. Supporting Information, figure S2 shows that the agreement is good over a range of scan rates. Moreover, we note that the values of E^0_{OH} and E^0_{HR} determined from fitting the low potential part of the CV, −224 and −292 mV at pH 6, are close to those determined in potentiometric experiments, −264 and −270 mV at pH 6.4, respectively.[24]

Phenomenological Parameter E_{switch}. In their studies of the anaerobic inactivation of hydrogenases Armstrong and co-workers have defined and used a phenomenological parameter called E_{switch}, the potential of the first inflection point on the return scan of the voltammograms[17] (see Figure 1).

To evaluate the robustness of E_{switch}, we compared the shape of the voltammograms recorded with different experimental parameters. As noted before,[17] we observed that the oxidative potential limit of the CV has little effect on E_{switch} (Supporting Information, Figure S3). However, the experiments in Figure 6A show that the value of E_{switch} is very dependent on scan rate: the four CVs were recorded successively with the same film of hydrogenase, at 4 different scan rates, from 6 mV/s down to 0.3 mV/s. Film desorption is the reason the current decreases from scan to scan (recording these four CVs took two hours). Panel B shows as red circles the corresponding values of E_{switch} plotted against scan rate. At high scan rate, E_{switch} decreases by about 75 mV per decade of scan rate (at T = 40 °C, pH 6). Supporting Information, Figure S4 shows that E_{switch} is also proportional to the log of scan rate in the case of the standard (oxygen-sensitive) NiFe hydrogenase from *D. fructosovorans*.

The rate constant of reactivation increases as the potential is swept toward negative values (Figure 4), and, in the limit of fast scan rate, the reactivation on the return scan is observed when the time constant of relaxation $1/(k_I(E) + k_A(E))$ is equal to the "natural" time scale of the voltammetric sweep, $1/f\upsilon$, where $f = F/RT$ and υ is the scan rate. In the region of E_{switch}, $k_A(E)$ is greater than $k_I(E)$ and we therefore suggest that the value of E_{switch} is such that

$$k_A(E_{switch}) \approx f\upsilon \qquad (16)$$

Using the empirical dependence of k_A on E determined using the two-step method (eq 12), we find

$$E_{switch} \approx \frac{1}{f\alpha} \ln \frac{k_0 \exp(\alpha f E^0)}{f\upsilon} = E^0 + \frac{1}{f\alpha} \ln \frac{k_0}{f\upsilon} \qquad (17)$$

This is plotted as a black line in Figure 6B. The measured values of E_{switch} match perfectly those predicted by eq 17 at high scan rates, which demonstrates that, in this limit, E_{switch} is defined by the kinetics of the reactivation and the scan rate. The slope of E_{switch} against ln (υ) is simply $-1/f\alpha$ (−75 mV per decade of scan rate at 40 °C, using the value of $\alpha = 0.8$ at pH 6, determined by fitting the data in Figure 4 to eq 12). Therefore, a −75 mV shift in E_{switch} would result from decreasing k_A 10-fold. This is important for comparing the values of E_{switch} of different hydrogenases.

We carried out numerical simulations to examine how the value of k_I affects the CVs. We observed that the shape of the voltammogram depends on k_I, in agreement with the results of Limoges et al.,[27] but the value of E_{switch} does not (data not shown). This is because k_I is much lower than k_A in the region of potential where the activity switches on.

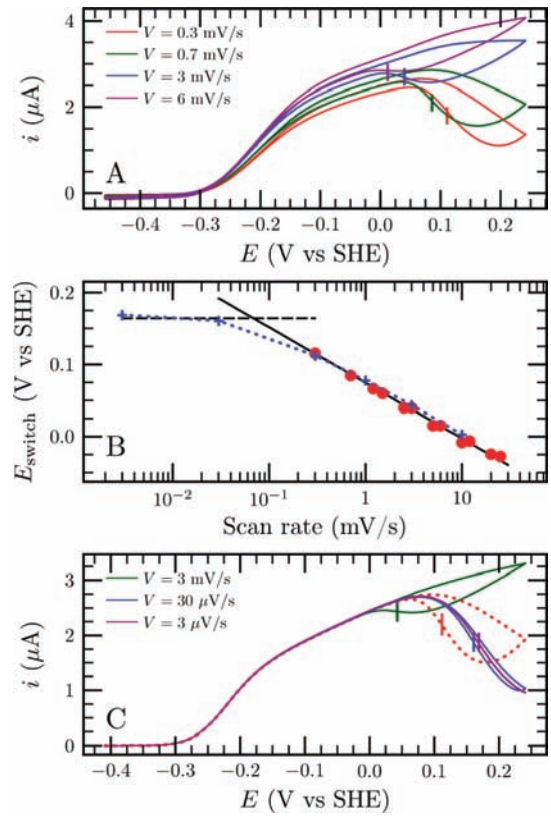

Figure 6. Influence of the scan rate on the value of E_{switch}. Panel A: cyclic voltammograms obtained under conditions similar to those of figure 5 for different values of the scan rate. Conditions: pH 6.1, 40 °C, ω = 4 krpm. Panel B: change in E_{switch} against scan rate. The red circles are the values determined from CVs such as those in Panel A, the black solid line is the prediction of eq 17, the black dashed line is that of eq 18 and the blue crosses connected by dashed segments are the values determined from simulated voltammograms, such as those shown in panel C. Panel C: the dashed line is the simulation shown in Figure 5, the other voltamograms were calculated using the same parameters as in Figure 5, except for the scan rates which we indicated in the inset.

We expect that the above reasonning should fail when the scan rate is so small that steady-state is achieved. This occurs at $v \ll k_I/f$, that is at scan rates well below 0.1 mV/s ($k_I \approx 2.10^{-3}$ s^{-1} for the data at pH 6 in Figure 4). To check this, we used the calculated voltammogram in Figure 5 as a reference and we examined how changing the scan rate affects the waveshape (panel C) and the value of E_{switch} (crosses connected by a dotted blue line in panel B). Only at very small scan rate (blue and purple CVs calculated for $v = 30$ and 3 μV/s respectively) does the value of E_{switch} become independent of scan rate. Since in this limit, there is hardly any hysteresis (the conversion between active and inactive forms is in a steady state), we conclude that eq 17 applies in all practical cases.

Although reaching steady-state would require unreasonnably small scan rates, it is interesting to discuss the meaning of E_{switch} in the steady-state limit. If $E_{switch}(v \to 0)$ is in a range of potential where $i(E)$ reaches a plateau,[37] its value is simply obtained by calculating the position of the inflection point of $A_\infty(E)$ (cf. eqs 4) using eqs 11 and 12:

$$E_{switch}(v \to 0) = \frac{1}{f\alpha} \ln \frac{k_0 \exp(\alpha f E^0)}{k_I + k_{A\,lim}} = E^0 + \frac{1}{f\alpha} \ln \frac{k_0}{k_I + k_{A\,lim}} \quad (18)$$

This limiting value of E_{switch} is plotted as a black horizontal dashed line in figure 6B. Importantly, E_{switch} does not tend to E^0 even in the low scan-rate limit.

Mechanism of the Anaerobic Inactivation and Activation. We now discuss the results of the chronoamperometric experiments in relation to the (in)activation mechanism.

An unexpected observation in Figure 4 is that k_A reaches a limiting value at high potentials. Under very oxidizing conditions and in the presence of hydrogen, both k_I and k_A tend to a limit, and so does the steady-state fraction of inactive enzyme: we have indeed observed that the activity does not drop to zero after a long poise at a high potential, and this is also the case of *A. vinosum* hydrogenase.[17] This suggests that under very oxidizing conditions, a slow process that is not driven by an electron transfer from the electrode activates the enzyme. It is tempting to assign it to a direct reaction with hydrogen. Indeed, Fernandez and co-workers reported in ref 38 that a lag phase in the assay of *Desulfovibrio gigas* hydrogenase disappears after long incubation with hydrogen (this is so even in the absence of redox mediators), suggesting that hydrogen can activate directly (albeit slowly) the NiB species. However, these experiments are not entirely conclusive, because the protein could have been activated upon reduction by traces of active enzyme, and preparations of *D. gigas* NiFe hydrogenase may have contained traces of cytochrome c_3, which is an efficient mediator. We observed that at pH 6, 40 °C, $k_{A\,lim}$ increases upon decreasing the hydrogen pressure from 1 atm. to 0.1 atm (Supporting Information, figure S5), which does not support the hypothesis that this reaction is caused by direct reaction of the enzyme with H_2. Further work is required to elucidate the reason that the rate of activation does not tend to zero at high potential.

The mechanism proposed in the literature for the anaerobic activation of NiFe hydrogenase involves the one electron reduction of the so-called NiB inactive species (probably $Ni^{III}OH$) into an intermediate state I ($Ni^{II}OH$), which loses a ligand to give the active state A (Ni^{II}); according to the electrochemical terminology, this is an "EC" mechanism, whereby the electrochemical step precedes the chemical step (Scheme 1).[17] The "$Ni^{II}OH$" intermediate is EPR silent, but in standard (oxygen-sensitive) NiFe hydrogenases, it has a characteristic FTIR signal. In contrast, the "$Ni^{II}OH$ " state could not be detected as an intermediate of the reduction of NiB in the case of *A. aeolicus* hydrogenase.[24]

Scheme 1. "EC" Mechanism Commonly Proposed for the Activation of the NiB State of Standard NiFe Hydrogenases

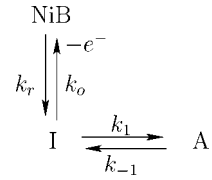

In the following, we consider three models of anaerobic (in)activation, two of which are based on the "EC" mechanism (Scheme 1), and we examine whether they are able to reproduce the available kinetic data regarding NiFe hydrogenases. This includes the potential dependence of $k_{tot} = k_I + k_A$, k_I and k_A obtained in the present work with the oxygen-tolerant *A. aeolicus* enzyme (Figure 4) and the literature values of k_{tot} obtained by Armstrong and co-workers with the standard NiFe hydrogenase from *A. vinosum*.[17] In Figure 7, the left and right colums show the *A. vinosum* data at pH 8.8, 45 °C, and *A. aeolicus* data at pH 8, 40 °C. The filled symbols, empty squares and empty triangles show k_{tot}, k_A, and k_I, respectively. Each row illustrates the best fits obtained by using one of the three models. In all cases, to account for the nonelectrochemical activation, we have added a rate constant $k_{A\,lim}$ to the predicted value of k_A.

First Model. To derive the (in)activation rate constants from Scheme 1, we shall assume that the oxidation and reduction rate constants k_o and k_r depend on E according to

$$k_o(E) = k_0\, e^{f(1-\alpha)(E-E^0)} \quad (19a)$$

$$k_r(E) = k_0\, e^{-f\alpha(E-E^0)} \quad (19b)$$

whereas k_1 and k_{-1} do not, and we use the key experimental observation that the reactivation is monoexponential. Indeed, Jones and co-workers observed that the activation of the NiB state of *A. vinosum* hydrogenase follows first-order kinetics.[17] In the case of *A. aeolicus* hydrogenase, this is supported by the perfect fit of the chronoamperometric data in Figure 3 to eq 10.

In the Supporting Information section S2, we show that the kinetic scheme 1 leads to monoexponential relaxation in only two cases. In the first one, NiB is in rapid equilibrium with its reduced counterpart I. This occurs if $k_r + k_o \gg k_1 + k_{-1}$.

This option can be ruled out from the data in Figure 4. Indeed, the assumption that NiB and I are in rapid equilibrium leads to

$$k_A = \frac{k_1}{1 + k_o(E)/k_r(E)} + k_{A\,lim} \quad (20a)$$

$$k_I = k_{-1} \quad (20b)$$

The term $1/(1 + k_o/k_r)$ gives k_A a sigmoidal dependence on E. The best fits to eqs 20 is illustrated on Figure 7A and B using red lines which are meant to overlay the *A. vinosum* and

(37) We demonstrate in the Supporting Information section S1 that if $E_{switch}(v \to 0)$ is in a region of potential where $i(E)$ varies linearly with E (instead of reaching a plateau), an additional small term contributes to the value of $E_{switch}(v \to 0)$.

(38) Fernandez, V.; Aguirre, R.; Hatchikian, E. *Biochim. Biophys. Acta* **1984**, *790*, 1–7.

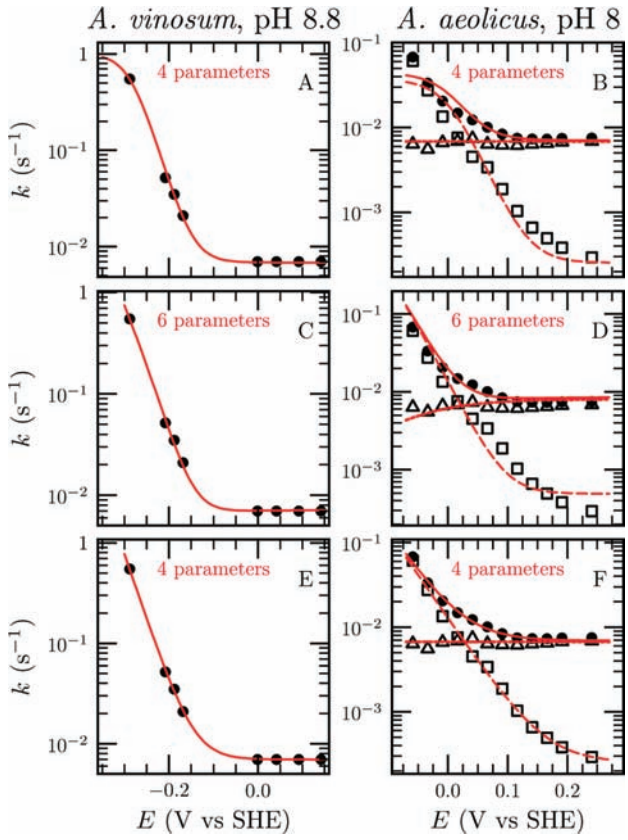

Figure 7. Rate constants of inactivation (k_I), activation (k_A), and interconversion ($k_{tot} = k_I + k_A$) as a function of potential, shown as open triangles, open squares and filled circles, respectively. The left column shows the *A. vinosum* data (pH 8.8, 45 °C) taken from the caption of Figure 7 and Figure 9 of ref 17 (we determined a single value for all potentials, which was estimated from the apparent slope on the log plot in figure 7C in ref 17 in the range $\log_{10}(i) = -6.2$ at $t = 105$ s to $\log_{10}(i) = -7.2$ at $t = 405$ s). The right column shows the values for *A. aeolicus*, replotted from figure 4 (pH 8, 40 °C). Red lines show the best fits of k_I, k_A and $k_I + k_A$ predicted by the models described in text (dotted, dashed and solid lines respectively); panel A and B: eqs 20; panel C and D: eqs 21; panel E and F: eqs 24 and 25. The number of adjustable parameters is indicated in each panel. Their values are listed in the Supporting Information section (Tables S1 to S3).

A. aeolicus data. Four pamameters needed to be adjusted (k_1, E^0, k_{-1}, $k_{A\,lim}$).

The agreement between eqs 20 and the *A. vinosum* data in Figure 7A is excellent but not very conclusive, since the data do not show the expected low potential limit of k_A ($k_A = k_1 + k_{A\,lim}$). The disagreement with the *A. aeolicus* data is more serious: the predicted dependence of k_A on E is too strong (dashed red lines and empty squares in panel B), and the model predicts a low potential plateau whereas the experimental values of k_A keep increasing exponentially as the potential is lowered.

Second Model. The second case that gives a monoexponential activation in the framework of the EC mechanism (cf. Supporting Information section S2) considers that the intermediate species I in scheme 1 reacts to form an active state much faster than it is formed upon reduction of the NiB state. This is so if k_o and k_1 are both much greater than $k_r + k_{-1}$. In that case

$$k_A = \frac{k_1 k_r(E)}{k_1 + k_o(E)} + k_{A\,lim} \qquad (21a)$$

$$k_I = \frac{k_{-1} k_o(E)}{k_1 + k_o(E)} \qquad (21b)$$

Scheme 2. Mechanism Proposed for the Formation of NiB in *A. aeolicus* Hydrogenase[a]

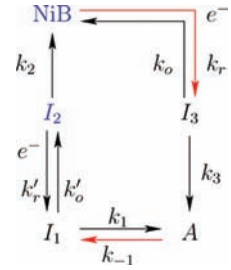

[a] I_1, I_2, and I_3 are transient species. Red arrows indicate the rate-limiting steps under the assumptions described in the text. The redox state of the Ni is +III in the states NiB and I_2, +II in all others. In eqs 19, E^0 is the reduction potential of the NiB/I_3 couple.

The best fits to eqs 21 shown in Figure 7C and D were obtained by adjusting six parameters k_0, E^0, α (cf. eqs 19), k_1, k_{-1}, and $k_{A\,lim}$.

The fit of ($k_I + k_A$) for *A. vinosum* in Figure 7C is again perfect, but when the values of k_I and k_A obtained with *A. aeolicus* hydrogenase are considered (Figure 7D), it becomes clear that the second model does not predict very well the variation of k_A in the high potential range. We shall see that the third model, considered below, does better with two fewer adjustable parameters.

Third Model. The EC model can reproduce the dependence of ($k_I + k_A$) on E, as suggested in ref 17 and shown in the left columns of Figure 7, but it cannot describe simultaneously the dependences of k_I and k_A of *A. aeolicus* hydrogenase (Figure 7B and D). The simplest solution to this dilemna is to assume that inactivation and reactivation proceed through two distinct routes, as depicted in Scheme 2. We suggest that, starting from the active state, a CE reaction forms an inactive state (I_2) which is unstable and irreversibly transforms into the NiB state that is observed in spectroscopy. The reactivation of NiB follows an EC mecanism, via the intermediate termed I_3.

Before we discuss the nature of these reactions, let us confirm that this model can predict the dependences of k_A and k_I on E. From Scheme 2, assuming that the species I_1, I_2, and I_3 do not accumulate, we obtain the following potential dependent rate constants

$$k_I = \frac{k_{-1} k'_o(E) k_2}{k_1 k_2 + k_1 k'_r(E) + k'_o(E) k_2} \qquad (22)$$

$$k_A = \frac{k_r(E) k_3}{k_3 + k_o(E)} + k_{A\,lim} \qquad (23)$$

Our goal here is not to determine all the above rate constants from the data in Figure 4 but to show that these equations can reduce to eqs 11 and 12, which reproduce exactly the data.

Let us assume that

(i) the reduction of NiB is coupled to the fast and irreversible formation of A ($k_3 \gg k_o(E)$ in the potential range of interest), so that

$$k_A = k_r(E) + k_{A\,lim} \qquad (24)$$

with $k_r(E) = k_0 \exp(-\alpha f(E - E^0))$, and

(ii) the formation of NiB follows up quickly the oxidation of I_1 to I_2 ($k_2 \gg k_r'(E)$) and the oxidation of I_1 makes the reaction

$A \rightarrow I_1$ irreversible ($k_o'(E) \gg k_1$) in the potential range of interest, so that

$$k_I = k_{-1} \quad (25)$$

This gives eqs 11 and 12 justification. The range of validity of the above approximations is discussed in the Supporting Information section S3. Only four parameters need to be adjusted to obtain the fits to eqs 24 and 25 shown on the bottom row of Figure 7: α, the product $k_0 \exp(\alpha f E^0)$, k_{-1}, and $k_{A\,lim}$.

Summary of Conclusions

Two-Step Method for Measuring (In)Activation Rate Constants. Electrochemical methods have been very instrumental for studying the inactivation reactions of hydrogenases.[10] This technique makes it easy to detect the (in)activation from the peculiar shape of the voltammograms[17,27] (Figure 1) or to measure rate constants by monitoring the relaxation of activity that follows a potential step. Here, we have proposed a novel two-step method, illustrated in Figure 2, for measuring the "true" activation and inactivation rate constants defined in eq 1, whereas the strategy that consists in fitting exponential relaxations only returns the sum of the two.[17,22] We have applied this method to *A. aeolicus* NiFe hydrogenase I (Figure 3) and by varying the experimental conditions, we were able to determine how these two rate constants depend on electrode potential, pH, and hydrogen concentration (Figure 4).

We have used these original data to demonstrate the relation between the (in)activation rate constants and the shapes of the voltammograms (Figures 5 and 6) and to test the (in)activation reaction scheme that has been proposed for standard NiFe hydrogenases.[17]

Understanding the Voltammetry. Modeling the potential dependence of k_I and k_A allowed us to simulate the cyclic voltammograms (CVs) recorded at a very slow scan rate (Figure 1). As explained before,[17,27] the pronounced hysteresis is caused by the transformation of the active site into the inactive NiB state as the conditions become very oxidizing, while the enzyme reactivates on the backward scan. Instead of simulating the voltammetry from a reaction scheme,[27] we used a semiempirical approach, which combines the steady-state current response of the fully active enzyme extrapolated from the low potential part of the data, and the time-dependent fraction of active enzyme determined by a numerical procedure which uses the (in)activation rate constants in Figure 4. The agreement between the simulations and the data is excellent (Figure 5 and Supporting Information, figure S2).

Since such voltammograms are very often used to diagnose the inactivation of hydrogenases, it was interesting to learn to interpret the CVs by finding out whether and how they are affected by the experimental and kinetic parameters. Of outstanding interest is the meaning of E_{switch}, the value of the electrode potential which produces the fastest increase in activity as the potential is scanned down.

Our results show that E_{switch} is not the reduction potential of the NiB species, even in the limit of very small scan rate (eq 18). When the scan rate is high enough that the voltammetry departs from steady state (that is, above 0.1 mV/s in the case of *A. aeolicus*, see Figure 6B), E_{switch} is defined by the ratio of scan rate over activation rate constant (eq 16). Equation 17 relates E_{switch} to a reduction potential (E^0) which cannot be unambiguously measured by analyzing the electrochemical data. The fundamental reason for this is that the rate of formation of NiB is independent of potential, and the rate of reactivation keeps increasing exponentially as the potential is lowered (Figure 4); when the latter is fitted to $k_A(E) = k_0\ e^{-\alpha f(E-E^0)}$, the two parameters k_0 and E^0 cannot be determined independently.

We demonstrated (Figure 6) that E_{switch} is actually the potential at which the activation rate constant equates the reciprocal of the natural time constant of the voltamogram ($k_A(E_{switch}) = f\upsilon$, $f = F/RT$). This explains several earlier observations: (i) The E_{switch} value of *A. aeolicus* (50 ± 20 mV at pH 7, 0.3 mV/s) does not match the reduction potential of the NiB species determined in a spectroelectrochemical FTIR titration of the same enzyme (−105 mV at pH 7.4[24]). (ii) The E_{switch} values of oxygen-tolerant enzymes are about 200 mV greater than that of standard hydrogenases. According to eq 17 a 10-fold increase in k_A shifts E_{switch} about 80 mV up; therefore, the higher value of E_{switch} is ultimately caused by the reactivation being about 3 orders of magnitude faster. This is fully consistent with the chronoamperometric results: at −208 mV, pH 8.8, 45 °C the enzyme from *A. vinosum* activates at a rate of $k_A = 5.2 \times 10^{-2}$ s^{-1} (caption of Figure 9 in ref 17), whereas the extrapolation of the *A. aeolicus* data at the same potential, at pH 8, 40 °C, gives $k_A \approx 10\ s^{-1}$.

Of course, thermodynamics may contribute to making the rate of activation faster, but since the reduction potential of NiB cannot be determined from the PFV data, the information must be obtained from potentiometric titrations. The reduction potential of NiB in *R. eutropha* has not been determined, but the reduction of NiB in *A. aeolicus* occurs at −105 mV at pH 7.4.[24] This is actually very similar to the value of −115 mV for *A. vinosum* at pH 8.[39] Therefore, in this case, the difference between the rates of activation of the two enzymes does not come from the reduction potential in eq 12, but from the prefactor. This term is an effective quantity that depends on the properties of the electronic relays that connect the active site to the electrode,[40] and we speculate that these are very different in the two enzymes. This may be the key to oxygen tolerance in hydrogenases.

The parameter E_{switch} has also been used in a qualitative manner to compare the "ease" with which hydrogenases activate[22,28,41] and our analysis supports this, provided the data are recorded at the same scan rate.

From the Kinetics of Activation to the Reaction Mechanism. Being able to determine independently the activation and inactivation rate constants (only their sum was measured in earlier investigations) provides fresh data which can be confronted to (in)activation reaction schemes. We showed that the data do not support the hypothesis that the NiB state is formed in a "CE" reaction, whereby ligand release precedes electron transfer, and reactivation proceeds via the reverse route (Scheme 1). Instead, we proposed the alternative mechanism in Scheme 2, which makes it possible to fit the (in)activation rate constants by adjusting two fewer parameters than the EC model (Figure 7F), and is based on assumptions that are fully consistent with the information gained from spectroscopic studies.[24] According to Scheme 2, the inactivation follows the $A-I_1-I_2-NiB$ pathway. The reactivation pathway, $NiB-I_3-A$,

(39) Coremans, J. M. C. C.; van der Zwaan, J. W.; Albracht, S. P. J. *Biochim. Biophys. Acta* **1992**, *1119*, 157–168.
(40) Léger, C.; Lederer, F.; Guigliarelli, B.; Bertrand, P. *J. Am. Chem. Soc.* **2006**, *128*, 180–187.

is not the reverse of the forward reaction series of events. The reaction scheme that Limoges and Savéant used for calculating voltammograms like that in Figure 1 also involved distinct activation and inactivation pathways (Scheme 3 in ref 27).

We tentatively assign these species using the information obtained from FTIR investigations: the active enzyme (A, or Ni^{II}) takes up one water molecule to produce the intermediate I_1 ($Ni^{II}H_2O$) which is oxidized to I_2 ($Ni^{III}H_2O$). Fast deprotonation gives NiB ($Ni^{III}OH$). Only the latter can be isolated. The slow one-electron reduction of NiB gives I_3 and the fast and irreversible loss of the bridging hydroxo follows up to give back the active state. That only two species accumulate to a significant extent (A and NiB) explains that the relaxation of activity is always monoexponential. The above mechanism is consistent with the fact that no intermediate between A and NiB is observed in spectroelectrochemical titrations of *A. aeolicus* hydrogenase.[24] This contrasts with standard hydrogenases, and therefore it is yet to be determined whether the mechanism in Scheme 2 is specific to *A. aeolicus* hydrogenase (and probably to the other oxygen-tolerant enzymes)[21,22,41] or if it applies to mesopholic hydrogenases as well. It is not yet possible to settle this issue, because only the sum $k_I + k_A$ has been determined in earlier studies of *A. vinosum*, and the discussion of the panels in the left column of Figure 7 shows that this experimental information alone does not allow to discriminate the different reaction mechanisms.

Methods

The soluble fragment of *A. aeolicus* NiFe hydrogenase I was purified as described previously[42] in a 50 mM Tris-HCl buffer pH 7.0 in the presence of 5−10% glycerol and 0.01% n-dodecyl-β-D-maltoside.

The experiments were carried out in a buffer mixture of MES (2-(*N*-morpholino)ethanesulfonic acid), CHES (2-[*N*-cyclohexylamino]-ethenesulfonic acid), TAPS (*N*-tris-[hydroxymethyl]methyl-3-aminopropanesulfonic acid), HEPES (*N*-(2-hydroxyethyl)-piperazine-*N*′-[2-ethanesulfonic acid]) and sodium acetate (5 mM each) and 0.1 M NaCl. The temperature and pH are indicated in each caption.

PFV (cyclic voltammetry and chronoamperometry) were carried out in a glovebox filled with N_2. The electrochemical equipment was described previously.[26,5] The enzyme was adsorbed by painting the freshly polished rotating disk graphite electrode (area ≈ 5 mm^2) with about 0. 5 μL of a stock solution of enzyme ($\sim$2 μM in the mixed buffer at pH 7) and let it dry for about one min.

The data were analyzed with an in-house program called SOAS, available via the Internet at http://bip.cnrs-mrs.fr/bip06,[43] which embeds the ODRPACK routine for nonlinear regression.[44] The contribution of the capacitive current in chronoamperometry experiments was removed by subtracting a blank, as illustrated in Supporting Information, figure S4.

All potentials are quoted with respect to the standard hydrogen electrode (SHE).

Acknowledgment. We thank Maria-Eirini Pandelia, Wolfgang Lubitz, Elisabeth Lojou, Sébastien Dementin, Pierre-Pol Liebgott, and Carole Baffert for fruitful discussions. We thank S. Dementin and P. P. Liebgott for preparing the sample of *D. fructosovorans* NiFe hydrogenase[5] which we used for the experiments in the Supporting Information, Figure S4. Our work is funded by the CNRS, CEA, ANR, Aix-Marseille Université, and the City of Marseilles. We acknowledge support from the "pôle de compétitivité Capénergies".

Supporting Information Available: Supplementary sections S1−S3, supplementary figures S1−S5, and supplementary tables S1−S3. This material is available free of charge via the Internet at http://pubs.acs.org.

JA910685J

(41) Lukey, M. J.; Parkin, A.; Roessler, M. M.; Murphy, B. J.; Harmer, J.; Palmer, T.; Sargent, F.; Armstrong, F. A. *J. Biol. Chem.* **2010**, *285*, 3928−3938.

(42) Brugna-Guiral, M.; Tron, P.; Nitschke, W.; Stetter, K.-O.; Burlat, B.; Guigliarelli, B.; Bruschi, M.; Giudici-Orticoni, M. T. *Extremophiles* **2003**, *7*, 145–157.

(43) Fourmond, V.; Hoke, K.; Heering, H. A.; Baffert, C.; Leroux, F.; Bertrand, P.; Léger, C. *Bioelectrochemistry* **2009**, *76*, 141–147.

(44) Boggs, P. T.; Donaldson, J. R.; Richaard,; Schnabel, R. B. *ACM Trans. Math. Software* **1989**, *15*, 348–364.